Supramolecular Double-Helix Formation by Diastereoisomeric Conformations of Configurationally Enantiomeric Macrocycles

Avik Samanta,[#] Zhichang Liu,[#] Siva Krishna Mohan Nalluri, Yu Zhang, George C. Schatz, and J. Fraser Stoddart*

Department of Chemistry, Northwestern University, 2145 Sheridan Road, Evanston, Illinois 60208-3113, United States

S *Supporting Information*

ABSTRACT: Solid-state superstructures, resulting from assemblies programmed by homochirality, are attracting considerable attention. In addition, artificial double-helical architectures are being investigated, especially in relation to the ways in which homochiral small molecules can be induced to yield helical forms as a result of chiral induction. Herein, we report the highly specific self-assembly upon crystallization of a double-helical superstructure from an enantiopure macrocyclic dimer which adopts two diastereoisomeric conformations in a molar ratio of 1.5:1 in dimethyl sulfoxide. These two conformational diastereoisomers self-organize—and self-sort—in the crystalline phase in equimolar proportions to form two single-handed helices which are complementary to each other, giving rise to the assembly of a double helix that is stabilized by intermolecular $[C-H\cdots O]$ and $\pi-\pi$ stacking interactions. The observed self-sorting phenomenon occurs on going from a mixed-solvent system containing two equilibrating conformational diastereoisomers, presumably present in unequal molar proportions, into the solid state. The diastereoisomeric conformations are captured upon crystallization in a 1:1 molar ratio in the double-helical superstructure, whose handedness is dictated by the choice of the enantiomeric macrocyclic dimer. The interconversion of the two conformational diastereoisomers derived from each configurationally enantiomeric macrocycle was investigated in CD_3SOCD_3 solution by variable-temperature ^{1}H NMR spectroscopy (VT NMR) and circular dichroism (VT CD). The merging of the resonances for the protons corresponding to the two diastereoisomers at a range of coalescence temperatures in the VT NMR spectra and occurrence of the isosbestic points in the VT CD spectra indicate that the two diastereoisomers are interconverting slowly in solution on the ^{1}H NMR time scale but rapidly on the laboratory time scale. To the best of our knowledge, the self-assembly of such solid-state superstructures from two conformational diastereoisomers of a homochiral macrocycle is a rare, if not unique, occurrence.
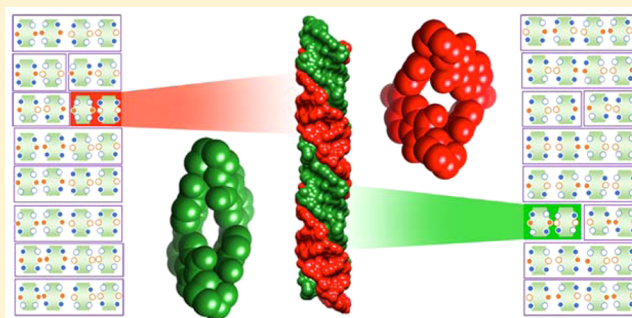
INTRODUCTION

The imaginations of scientists are often captured by chance events that occur in nature or surface in art[1] and/or architecture.[2] Every so often, comparisons with day-to-day objects and phenomena help chemists in their understanding of nature and in their explanations of emergent behavior that is being recognized more and more in chemistry. Naturally occurring hierarchies constructed by living organisms which find their chemical pedigrees in molecular (covalent) and supramolecular (noncovalent) morphogenesis are presently a source of detailed inquiry[3] in the physical and biological sciences. There is an expectation[4] that these emergent phenomena will spawn novel materials with unanticipated properties. Helicity is a topographical motif which is eye-catching from an aesthetic point of view.[5] The elegance surrounding the three-dimensional (3D) tertiary structures and recognition properties of naturally occurring helical polymers, such as the α-helix[6] adopted by polypeptides in many proteins and the double helix in DNA,[7] has encouraged chemists to design and synthesize artificial helical oligomeric and polymeric

superstructures.[8] Artificial double-helical architectures have attracted much attention,[9] especially in relation to the ways in which they can be constructed and induced to yield a particular chiral sense. Considerable effort has been invested[5,10] by chemists into mimicking the helical geometry of DNA based on molecular and supramolecular approaches. In DNA, the interacting base pairs are orthogonal to the deoxyribose phosphate backbones, and $\pi-\pi$ stacking between base-pair layers defines the double-helical geometry. So far, only a few structural motifs have been engineered for the coherent design and synthesis of artificial double helices based on supramolecular interactions, i.e., metal coordination,[9a,c,11] interstrand hydrogen-bonding,[12] aromatic–aromatic interactions,[13] and strain-induced twisting.[14] As supramolecular chemistry[15] has become a vastly diverse field, macrocycles have been singled out for the successful construction of a wide array of 3D superstructures with increasing complexity.[16] Recently, we
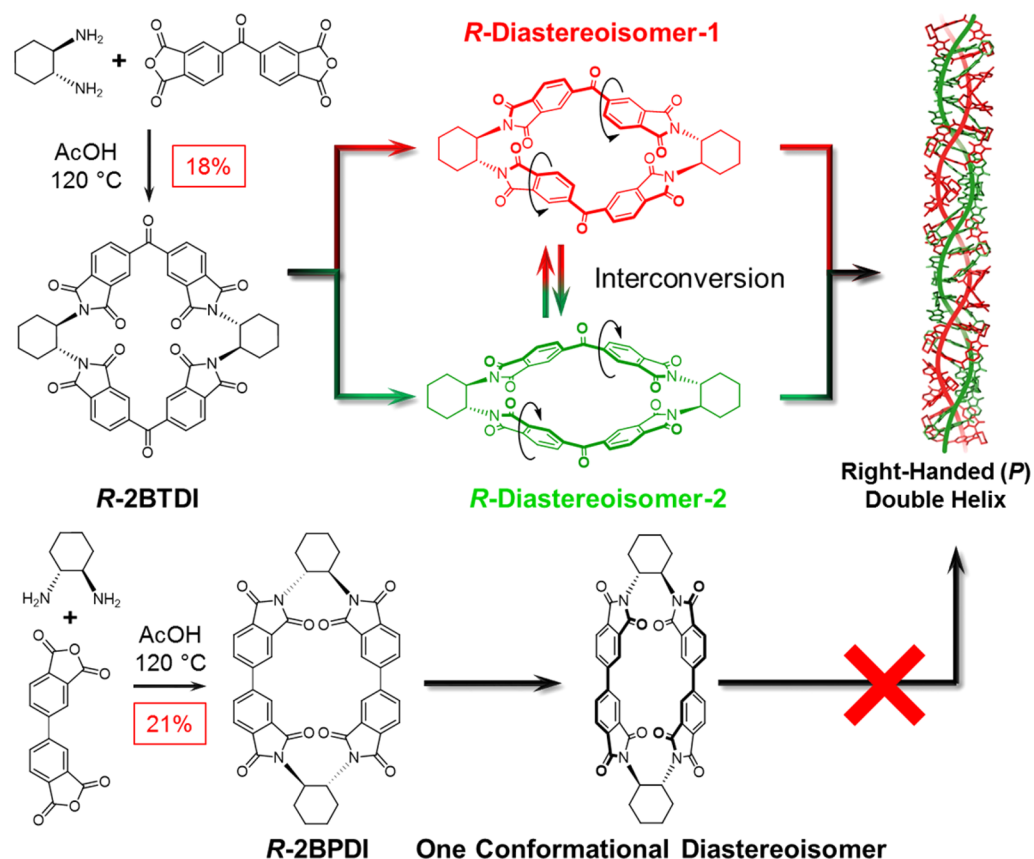
Figure 1. Synthesis of **R-2BTDI** and **R-2BPDI** along with a schematic representation of the self-assembly upon crystallization of a complementary supramolecular double helix, which turns out to be an equimolar mixture of the two conformational diastereoisomers of **R-2BTDI**.

described[17] the emergent behavior of chiral triangular macrocycles composed of naphthalene diimide units in the formation of single-handed supramolecular helices by dint of intermolecular $\pi-\pi$ stacking in the presence of linear I_3^- anions.

On the other hand, molecular chirality plays a significant role in self-assembly processes, giving rise to helical 3D superstructures.[18] Since Pasteur's famous chiral sorting experiment,[19] also known as "*spontaneous resolution*",[20] the breaking of the symmetry in racemic mixtures of enantiomers has been found in several cases, during (i) crystallization[21] and (ii) self-assembly on solid surfaces[22] and (iii) other well-ordered structures.[23] In recent years, the general term "*self-sorting*" has been invoked[24] to describe the high-fidelity recognition between molecules or ions within a mixture, where their affinities can be either for others—*social self-sorting*[25]—or for themselves—*narcissistic self-sorting*.[26] Molecular building blocks of different size, shape, rigidity, or chirality can self-sort into distinct supramolecular architectures while maximizing noncovalent interactions, such as hydrogen bonding[27] and $\pi-\pi$ stacking.[28]

Herein, we describe the serendipitous discovery of a solid-state double-helical superstructure composed of two conformational diastereoisomers of a homochiral redox-active dimeric macrocycle. The fundamental basis for this 3D helical architecture is a self-sorting phenomenon which dictates the equimolar capturing of two conformational diastereoisomers in the solid state, starting from an equilibrating mixture of these diastereoisomers in solution. This observation constitutes an example of emergent behavior[29] in a complex system passing from solution into the solid state. The generation of

supramolecular chirality through chiral induction[30] in the crystalline state is a consequence of the four stereogenic centers (configurational chirality) in the starting macrocycles. Two equilibrating conformational diastereoisomers of the dimeric macrocycle form two complementary single helices which are entwined with each other through multiple hydrogen-bonding and aromatic interactions, giving rise (Figure 1) to a supramolecular double helix in the solid state. We happened upon this event having synthesized two enantiopure chiral cyclophanes, each consisting of two cofacially assembled benzophenone-3,3',4,4'-tetracarboxylic diimide (BTDI) units, held together by two chiral cyclohexano linkers. Derivatives of BTDI are a well-known class of electron-deficient aromatic compounds that have found numerous applications, such as in gas separation,[31] dentistry,[32] heat-resistant organoclay hybrids,[33] and membranes with antimicrobial properties.[34] Both of the enantiomeric cyclic dimers—namely, (*RRRR*)-**2BTDI** and (*SSSS*)-**2BTDI**, referred to in this paper simply as **R-2BTDI** and **S-2BTDI**, respectively—exist in two diastereoisomeric conformations at room temperature, both in solution phase and in the solid state. Equimolar proportions of the two diastereoisomeric conformations of **R-2BTDI** assemble (Figure 1) into a right-handed double-helical superstructure, while the corresponding diastereoisomeric conformations of **S-2BTDI** assemble into a left-handed double-helical superstructure. For the sake of comparison, we synthesized another pair of enantiomeric cyclic dimers—without the ketonic C=O groups between the phenylene rings—composed of 3,3',4,4'-biphenyltetracarboxylic diimide (BPDI) units—namely, **R-2BPDI** (Figure 1) and **S-2BPDI**. In contrast with the two diastereo-
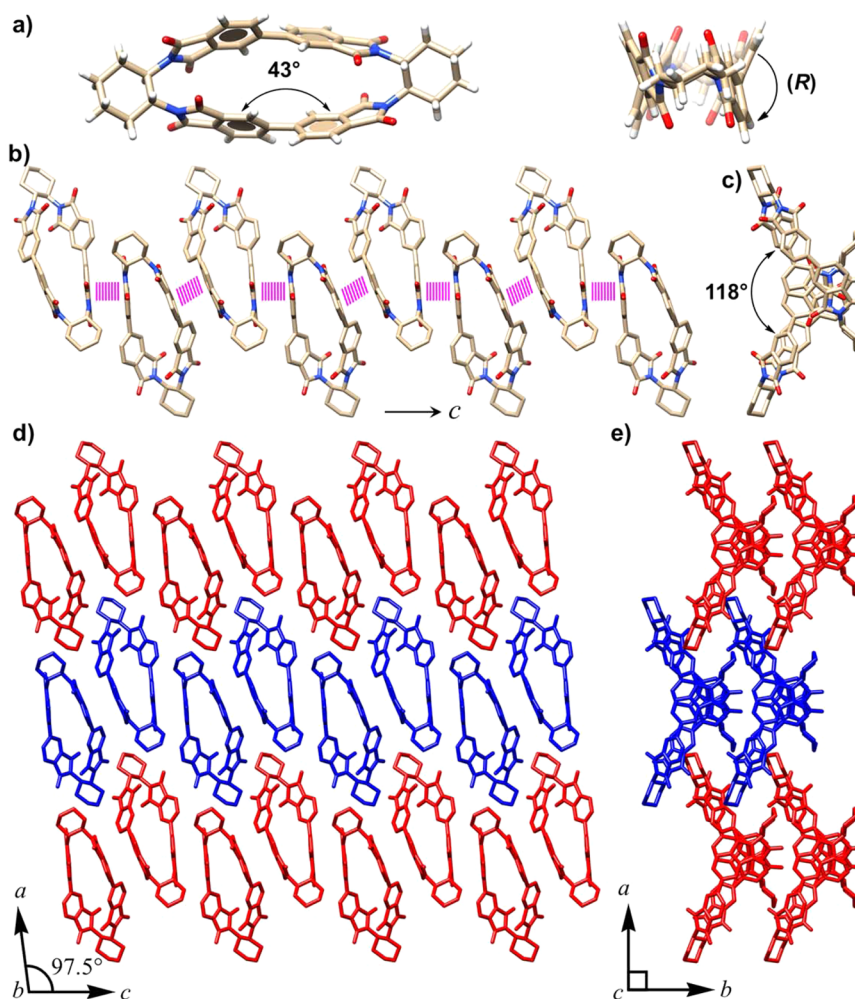
Figure 2. Single-crystal X-ray (super)structure of **R-2BPDI**. (a) Tubular representation of **R-2BPDI**. Left: Top view showing the flattened geometry and the dihedral angle of 43° associated with the biphenyl groups. Right: Side-on view indicating the (R)-axial chirality of the biphenyl groups. (b,c) Top and side-on views of the 1D roof-shaped non-helical superstructure formed by means of π−π interactions between benzoimides on adjacent macrocycles stacked along the c-axis alternatingly with a crossing angle of 118°. The magenta hatched lines describe the π−π interactions. Protons are omitted for the sake of clarity. (d,e) Two views of the packing of the 1D roof-shaped superstructure along the b- and c-axes. For the sake of clarity, adjacent 1D superstructures are depicted alternatingly in blue and red.

isomeric conformations observed for both **R-2BTDI** and **S-2BTDI**, we observed only one conformational diastereoisomer for both **R-2BPDI** and **S-2BPDI** at room temperature. In recent years, we have investigated cyclical through-space electron sharing among neighboring redox-active units confined in several cyclic geometries, including a rigid dimer,[35] a triangle,[17,36] and a square.[37] When the redox properties of the macrocycles **R-2BTDI** and **R-2BPDI** were investigated, electronic communication[38] was observed in solution, in contrast with those of their monomeric counterparts **BTDI-ref** and **BPDI-ref**. The electronic coupling between the redox-active moieties (BTDI or BPDI) in **R-2BTDI** and **R-2BPDI** gives six and four accessible redox states, respectively.

RESULTS AND DISCUSSION

Synthesis. The pairs of pure enantiomeric chiral cyclic dimers were synthesized in one-pot condensations between commercially available (RR)- or (SS)-trans-1,2-cyclohexane-diamine and a couple of dianhydride derivatives. The condensation between biphenyltetracarboxylic dianhydride (BPDA) and (RR)- or (SS)-trans-1,2-cyclohexanediamine in refluxing acetic acid afforded (Figure 1, Schemes S3 and S4) a

pair of pure enantiomeric dimers—namely, **R-2BPDI** and **S-2BPDI**—in 21 and 20% yields, respectively. Both **R-2BPDI** and **S-2BPDI** were characterized by electrospray ionization high-resolution mass spectrometry (ESI-HRMS), which confirmed the presence of the species $[M + Cl]^-$ at m/z = 779.1917 and 779.1905 (calculated 779.1909), respectively. Similarly, the condensation of an equimolar mixture between benzophenone-3,3′,4,4′-tetracarboxylic dianhydride (BTDA) and (RR)- or (SS)-trans-1,2-cyclohexanediamine in refluxing acetic acid gave (Figure 1, Schemes S1 and S2) the corresponding dimeric macrocycles—namely, **R-2BTDI** and **S-2BTDI**—in 18 and 16% yields, respectively. Characterization of both **R-2BTDI** and **S-2BTDI** was achieved by ESI-HRMS, which confirmed the presence of the species $[M + Cl]^-$ at m/z = 835.1805 and 835.1815 (calculated 835.1807), respectively. Two monomeric analogues—namely, **BPDI-ref** and **BTDI-ref**—were also prepared (Schemes S5 and S6), by the condensation of cyclohexylamine with BTDA and BPDA, respectively, and characterized. The purification of the macrocycles was achieved by flash silica chromatography, giving purities in excess of 99%.
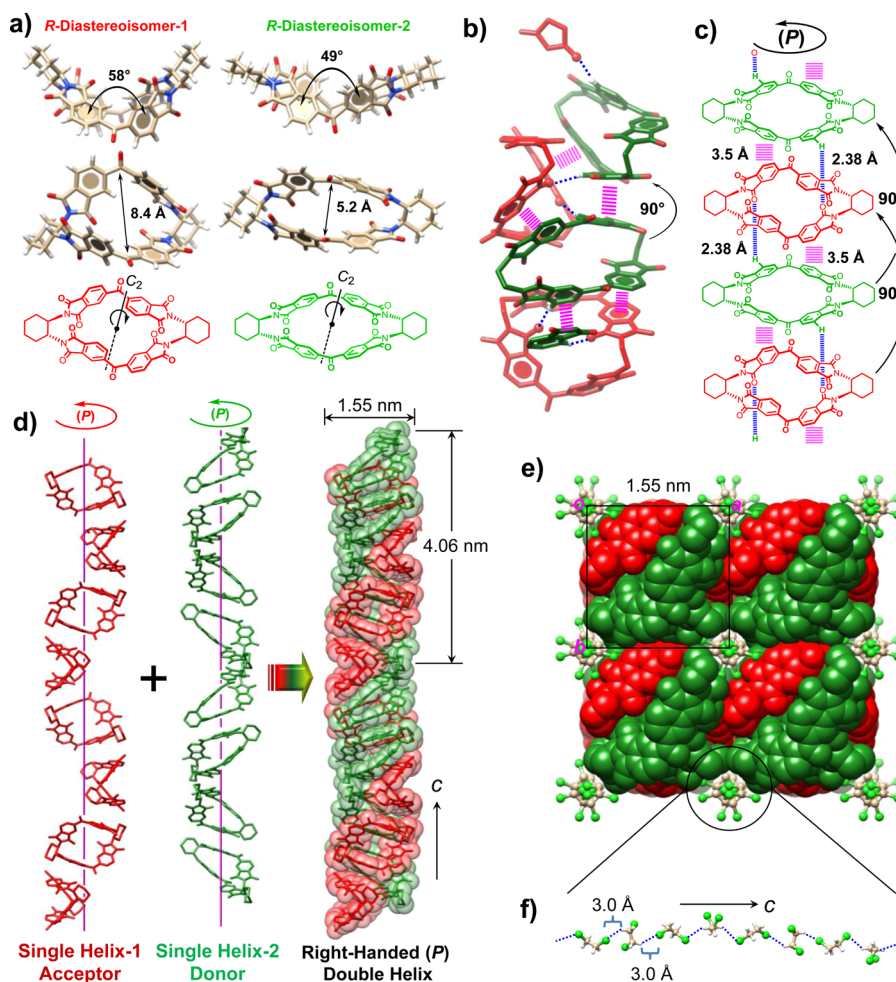
Figure 3. Single-crystal (super)structure of the double helix formed on crystallization of **R-2BTDI**. (a) Solid-state structures of **R-Diastereoisomer-1** (left) and **R-Diastereoisomer-2** (right) and their corresponding structural formulas: C, tan; H, white; O, red; N, blue. (b) Complementary noncovalent bonding interactions between two pairs of diastereoisomers and (c) a schematic structural representation. In (b) the O atoms of both the diastereoisomers are denoted in red, and the H atoms participating in [C−H···O] hydrogen-bonding for **R-Diastereoisomer-2** are shown in white. Blue dashed lines indicate the [C−H···O] hydrogen-bonding interactions, while magenta hatched lines describe the π−π stacking interactions between the two diastereoisomers. The atoms involved in hydrogen bonding are represented as balls. The black arrows indicate the counterclockwise relative rotation angles of 90° between adjacent **R-Diastereoisomer-1** and **R-Diastereoisomer-2**. The cyclohexano rings in (b) are omitted for the sake of clarity. (d) Solid-state superstructure of the complementary right-handed (P)-double helix assembled from the single (P)-helix-1 (red) of the hydrogen-bonding acceptor **R-Diastereoisomer-1** and the single (P)-helix-2 (green) of the hydrogen-bonding donor **R-Diastereoisomer-2**. The pitch length and diameter are indicated in black. (e) Space-filling representation of the view along the c-axis of the superstructure of the double helix. The solvent chains are shown in ball-and-stick representations. (f) The [C−H···Cl] hydrogen-bonded ClCH$_2$CH$_2$Cl chain: C, tan; H, white; Cl, green.

X-ray Diffraction Analysis. Single crystals of enantiopure **R-2BPDI** and **R-2BTDI** suitable for X-ray diffraction (XRD) were obtained by slow vapor diffusion of n-hexane into a 4.0 mM solution of the corresponding macrocycle in ClCH$_2$CH$_2$Cl over the course of a week at 4 °C. It is worthy of note that a high yield (>95%) of the **R-2BTDI** crystals was obtained on crystallization, indicating that equilibration between its two diastereoisomers is occurring rapidly in solution at 4 °C. Single-crystal X-ray analysis reveals[39] that **R-2BPDI** (Figure 2a) adopts only one flattened C$_2$-symmetric conformation, with a separation of 4.6 Å between the two (R)-biphenyl moieties and a dihedral angle of 43° between the two benzoimides. These macrocycles stack up (Figure 2b) along the c-axis alternatingly with a crossing angle of 118° (Figure 2c) between adjacent units on account of intermolecular π−π stacking interactions between the adjacent benzoimides, resulting in a 1D non-helical roof-shaped superstructure (Figure 2c−e). On the other hand,

X-ray crystallographic analysis of **R-2BTDI** reveals[40] (Figure 3a) that the asymmetric unit is composed of two conformational diastereoisomers—namely, **R-Diastereoisomer-1** and **R-Diastereoisomer-2**, both having two-fold symmetry, with the C$_2$ axes passing through the center of both macrocycles—in a 1:1 ratio. The **R-Diastereoisomer-1** has a highly bent saddle shape, wherein two of the phenylene rings in each benzophenone moiety are in a *syn* orientation,[41] with a "dihedral angle" of 58° and a distance between the two ketonic C═O groups of 8.4 Å. By contrast, **R-Diastereoisomer-2** adopts a less bent saddle-shaped conformation—which can be obtained from **R-Diastereoisomer-1** by rotating the two diagonal outwardly inclined phenylene rings through 180°— wherein two phenylene rings in each benzophenone moiety are in an *anti* orientation,[42] with a "dihedral angle" of 49° and a distance between the two ketonic C═O groups of 5.2 Å. The torsional angles (Table S1) at comparable locations in the
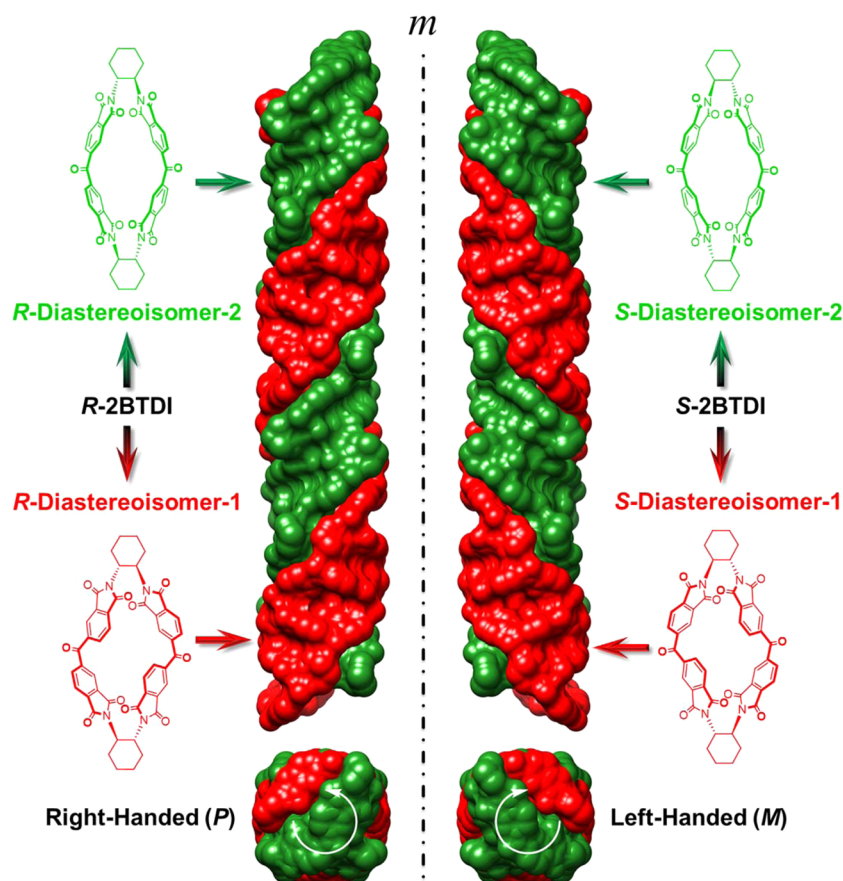
Figure 4. (*P*)- and (*M*)-double helices formed separately from the enantiomeric *R*-2BTDI and *S*-2BTDI, respectively. *R*- and *S*-Diastereoisomer-1, as well as their corresponding single helices, are depicted in red, while *R*- and *S*-Diastereoisomer-2, as well as their corresponding complementary single helices, are shown in green.

benzophenone units in **R-Diastereoisomer-2** are quite similar to those in the solid-state structure of pristine benzophenone[43] but rather different from the torsional angles of **R-Diastereo-isomer-1**. In the single-crystal superstructure, **R-Diastereo-isomer-1** and **R-Diastereoisomer-2** are engaged together through their concave faces to form a supramolecular dimer by means of a [C—H···O] hydrogen-bonding interaction ($d_{H···O}$ = 2.38 Å and $\theta_{C-H···O}$ = 166°) between an H atom on one of the outwardly tilted phenylene rings of **R-Diastereoisomer-2** and an inwardly pointed O atom on one of the imide groups of **R-Diastereoisomer-1**. These dimers then stack (Figure 3b,c) along the *c*-axis with a counterclockwise rotation of 90° relating them, resulting in an infinite right-handed (*P*) supramolecular double helix through discrete (i) [C—H···O] hydrogen-bonding interactions between an H atom on the diagonal outwardly tilted phenylene ring of **R-Diastereoisomer-2** and an O atom on the diagonal inwardly tilted imide group of **R-Diastereo-isomer-1** in adjacent dimers and (ii) π−π stacking interactions (~3.5 Å) between the inwardly tilted phenylene rings of both diastereoisomers in adjacent dimers. As a consequence, four dimers (four **R-Diastereoisomer-1** and four **R-Diastereo-isomer-2**, Figure 3d,e) form a complete helical pitch within this infinite helix—which constitutes a tetragonal unit cell—with a pitch length of 4.06 nm and a diameter of 1.55 nm. In this 1D superstructure, **R-Diastereoisomer-1**—which provides two O atoms on the diagonal imide groups as hydrogen-bonding acceptors—coils around the *c*-axis, to form an acceptor (*P*)-single-helix-1 (red), while **R-Diastereoisomer-2**—which

provides two H atoms on the diagonal phenylene rings as hydrogen-bonding donors—coils around the same axis, forming a complementary donor (*P*)-single-helix-2 (green). These two donor and acceptor complementary (*P*)-single helices continue to entwine tightly in the shape of a (*P*)-double helix, driven by complementary [C—H···O] and π−π interactions. In the *a*−*b* plane, these 1D double helices pack (Figure 3e) closely in a square arrangement with unit cell parameters *a* = *b* = 1.55 nm. The channels alongside these helices are filled up (Figure 3f) by [C—H···Cl] hydrogen-bonded ClCH$_2$CH$_2$Cl chains. This single-handed double-helical superstructure is reminiscent (Table S2) of the classical double-helical structure of DNA.[44] In addition to the (*P*)-double helix formed from **R-Diastereoisomer-1** and **R-Diastereoisomer-2** of **R-2BTDI**, the enantiomeric (*M*)-double helix was also obtained[45] from **S-Diastereoisomer-1** and **S-Diastereoisomer-2** of the enantiomer **S-2BTDI**. This observation highlights the fact that the helical sense of the double helix is determined (Figure 4) by the chirality of the macrocyclic building blocks—namely, **R-2BTDI** leads to a right-handed (*P*)-double helix, while **S-2BTDI** leads to a left-handed (*M*)-double helix. The dramatic change in shape of **R-2BTDI** and the solid-state superstructure compared with that of **R-2BPDI** indicates that the insertion of the ketonic C═O groups between the two pairs of benzoimide groups endows the macrocyclic diastereo-isomers of **R-2BTDI** with sufficient conformational flexibility to facilitate the assembly of the right-handed (*P*)-double helix on account of (i) the saddle-shaped geometry of the diastereo-
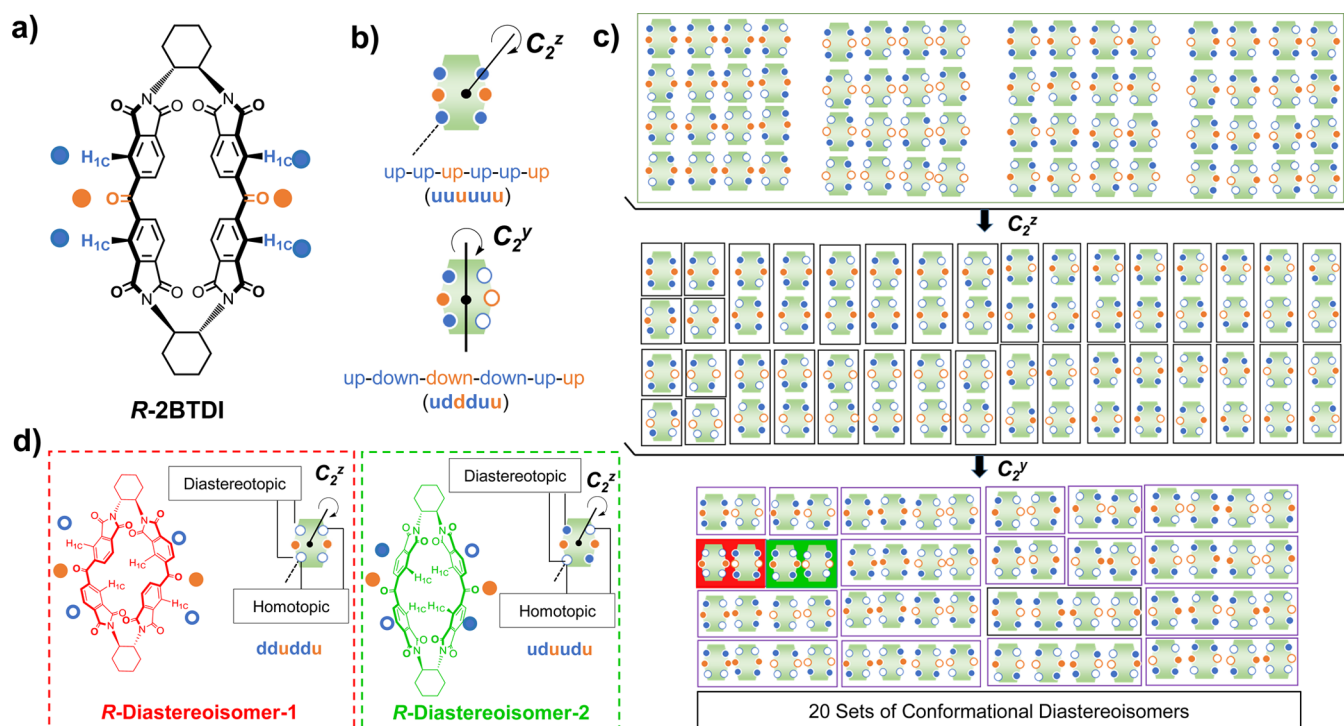
Figure 5. Conformational diastereoisomers of **R-2BTDI**. (a) Structural formula defining the up-up-up-up-up-up (**uuuuuu**) diastereoisomer of **R-2BTDI**. (b) Schematic representation of the **uuuuuu** and up-down-down-down-up-up (**uddduu**) conformations with their corresponding two-fold axes of symmetry defined. (c) Conformational distribution analysis dependent on the relative positions of the H_{1C} atoms and the ketonic C=O groups with respect to the plane of the paper. (d) Structural formulas of the two observed conformational diastereoisomers of **R-2BTDI** and their schematic representations.

isomeric macrocycles in **R-2BTDI** and (ii) the formation and interconversion of the two complementary macrocyclic diastereoisomers.

Conformational Analysis. Inspection of molecular models of the macrocycles reveals that the BTDI units in **R-2BTDI** (or **S-2BTDI**) are conformationally flexible, and so it is anticipated that a fleet of conformational diastereoisomers might be present. Conformational analysis (Figure 5a−c) was performed in an attempt to identify all the possible conformational diastereoisomers of **R-2BTDI** and then compare the results of the analysis with the experimental results. The dimeric macrocycle **R-2BTDI** (and **S-2BTDI**) has two BTDI units connected by two chiral cyclohexano rings. The stereogenic centers associated with the two cyclohexano rings can be defined as *RRRR* in the case of **R-2BTDI** and *SSSS* in the case of **S-2BTDI**. These stereogenic centers were omitted from the conformational analysis in order to simplify the representation (Figure 5b). In total, 20 possible conformational diastereoisomers were identified (Figure 5c) by (i) permuting the relative orientations of the isolated *ortho* hydrogen atoms (identified by the descriptors H_{1C} in Figure 5a) on the four phenylene rings with respect to the ketonic C=O groups connecting them and then (ii) taking into consideration the degeneracy associated with the analysis. When the H_{1C} atoms and the O atoms in the ketonic C=O groups are directed upward, they are labeled as **u** (solid circles, ●), and when they are oriented downward, they are designated as **d** (open circles, ○). Out of the 20 discretely different[46] conformational diastereoisomers, only two—**dduddu** (**R-Diastereoisomer-1**) and **uduudu** (**R-Diastereoisomer-2**)—were observed (Figure 5d) in solution, as evidenced by both ^{1}H and ^{13}C NMR spectroscopies, and in the solid state (Figure 3a), as evidenced

by single-crystal XRD analysis. This kind of coexistence of two conformational diastereoisomers in both solution and the solid state for wholly synthetic macrocycles is not so common.[47] Characterization of the two diastereoisomeric conformations in solution is challenging on account of their interconversion on the laboratory time scale at room temperature.[48]

NMR Spectroscopy. The ^{1}H NMR spectrum (Figures 6a and S1) of **R-2BTDI** recorded in CD_3SOCD_3 displays (δ 7.25−8.32 ppm) discrete resonances (red/green) in the downfield region characteristic of protons arising from two conformational diastereoisomers, indicating that interconversion between them is slow on the ^{1}H NMR time scale at room temperature. The aliphatic methine (CH) and methylene (CH₂) protons of the chiral cyclohexano linkers give rise to resonances (Figure S1) in the upfield regions at δ 4.35−4.60 and 1.30−2.81 ppm, respectively. Following detailed analyses of the 1D and 2D ^{1}H NMR spectra in the downfield regions, the signals corresponding to two conformational diastereoisomers (Figure 5d) were identified as (i) two sets of doublets and a sharp singlet (red), corresponding to the **dduddu** conformation (**R-Diastereoisomer-1**), and (ii) four sets of doublets and two sets of singlets (green), corresponding to the **uduudu** conformation (**R-Diastereoisomer-2**). The H_{1C} protons on the diagonally related phenylene rings in the case of both conformations, **dduddu** and **uduudu**, are homotopic (on account of the C_2^z axes), while the H_{1C} protons on the same BTDI units are diastereotopic with respect to each other (Figure 5d). In the case of the **dduddu** diastereoisomer, the diastereotopic H_{1C} protons could accidentally give rise to resonances having the same chemical shifts, since the stereogenic centers on the cyclohexano rings are distant from the aromatic protons in addition to the fact that all four of the
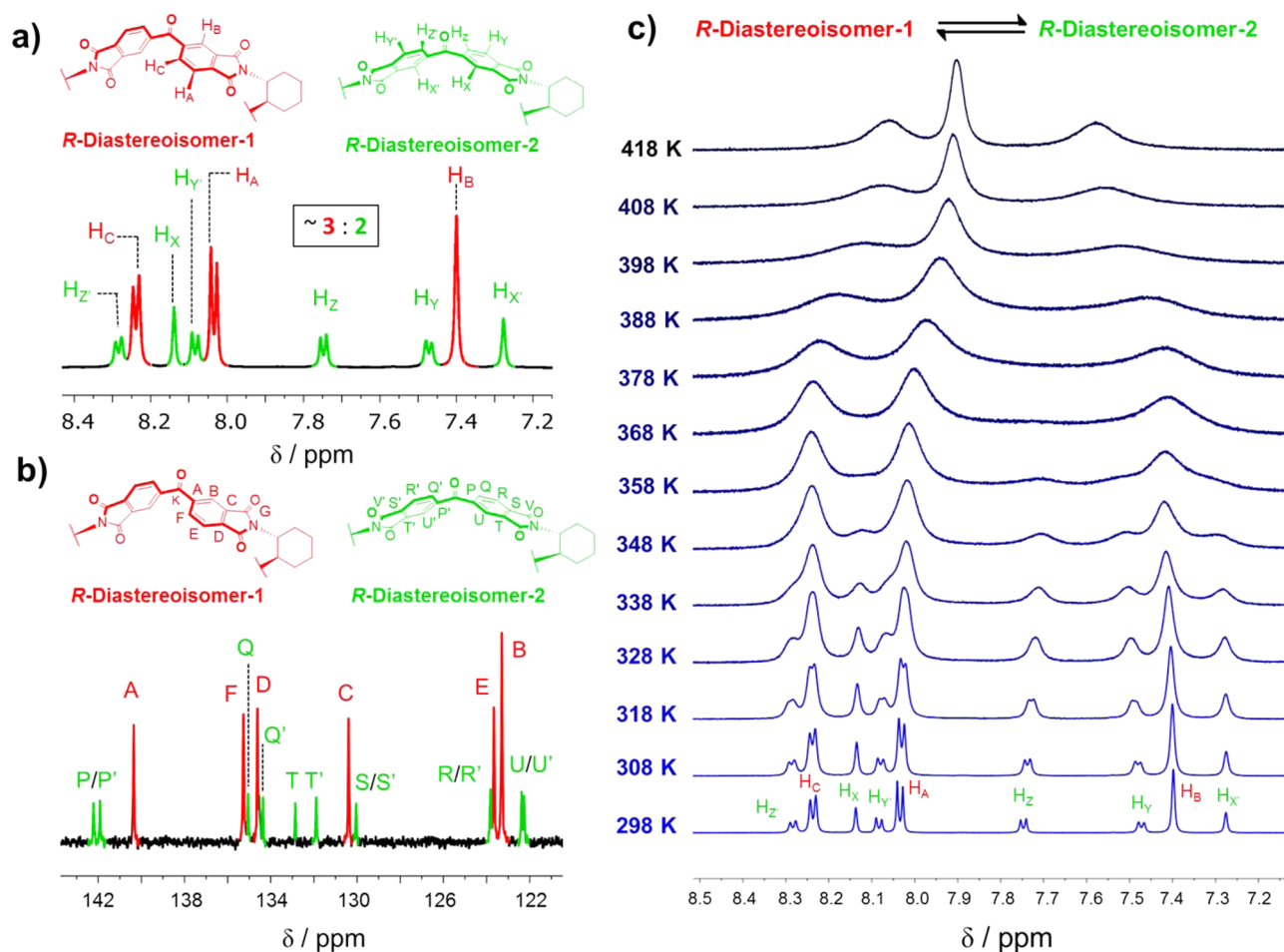
Figure 6. Partial ^1H and ^{13}C NMR spectra and dynamic NMR investigations in solution. (a) Annotated partial ^1H NMR spectrum (500 MHz, CD_3SOCD_3, 298 K) of the dimeric macrocycle *R*-2BTDI. The signals corresponding to the aromatic protons of the *R*-Diastereoisomer-1 and *R*-Diastereoisomer-2 are denoted in red and green, respectively. The ratio of *R*-Diastereoisomer-1 to *R*-Diastereoisomer-2 is 1.5:1 in CD_3SOCD_3, based on the integration of the red and green peaks. The full spectra, along with unambiguous assignments of the methine protons and the axial and equatorial protons of the cyclohexano linkers, are presented in the Supporting Information. (b) Annotated partial ^{13}C NMR spectrum (125 MHz, CD_3SOCD_3, 298 K) of the dimeric macrocycle *R*-2BTDI. The signals for the conformational diastereoisomers are denoted in red (for *R*-Diastereoisomer-1) and green (for *R*-Diastereoisomer-2). (c) Variable-temperature ^1H NMR spectra (600 MHz, CD_3SOCD_3) for *R*-2BTDI encompassing the aromatic region: the coalescence temperature for signals associated with *R*-Diastereoisomer-1 and *R*-Diastereoisomer-2 protons [(H_C, $H_{Z'}$, and H_Z), (H_A, $H_{Y'}$, and H_Y), or (H_X, H_B, and $H_{X'}$)] is observed at 378 K.

H_{1C} protons are oriented *syn* to each other and pointing in opposite directions with respect to the ketonic C=O groups. Additionally, the H_{1C} protons in conformation **dduddu** are expected[49] to exhibit upfield shifts of their resonances with respect to the other two phenylene ring protons on account of their orientations (Figure 5d) in relation to the ketonic C=O groups. Hence, in the ^1H NMR spectrum (Figure 6a) of *R*-2BTDI, the chemical shifts (peaks represented in red) of the singlet associated with H_B resonate at δ 7.40 ppm and the two doublets corresponding to H_A and H_C resonate at δ 8.05 and 8.25 ppm, respectively, and arise from *R*-Diastereoisomer-1. On the other hand, in the diastereoisomer **uduudu** (*R*-Diastereoisomer-2), the diastereotopic H_{1C} protons associated with the BTDI units are *anti* to each other, and only two out of the four are oriented in the same direction as the ketonic C=O groups, giving rise (green) to two singlets for two sets of diastereotopic H_{1C} protons and four doublets for the other eight phenylene ring protons.[50] Hence, in the ^1H NMR spectrum (Figure 6a) of *R*-2BTDI, two singlets corresponding to $H_{X'}$, *anti* to the ketonic C=O groups, and H_X, *syn* to the

ketonic C=O groups, were observed at δ 7.27 and 8.14 ppm, respectively. The other phenylene ring protons, $H_{Y'}$ and $H_{Z'}$, *syn* to the ketonic C=O groups, resonate as two doublets at δ 8.07 and 8.30 ppm, respectively, while the other two protons, H_Y and H_Z, *anti* to the ketonic C=O groups, resonate as doublets at δ 7.48 and 7.75 ppm, respectively. The coexistence of *R*-Diastereoisomer-1 and *R*-Diastereoisomer-2 in solution is also confirmed in the ^{13}C NMR spectrum (Figures 6b and S2) at room temperature, where six distinct peaks are observed from δ 122.4 to 142.3 ppm for phenylene ring carbons in *R*-Diastereoisomer-1 and 12 peaks for the phenylene ring carbons of *R*-Diastereoisomer-2. The ratio of *R*-Diastereoisomer-1 to *R*-Diastereoisomer-2 was found to be 1.5:1 in CD_3SOCD_3. Both ^1H and ^{13}C NMR spectra (Figures S5 and S6) of *S*-2BTDI are identical with those of its enantiomer.

In order to probe the kinetics associated with the equilibration in solution between *R*-Diastereoisomer-1 and *R*-Diastereoisomer-2 in *R*-2BTDI, we have carried out dynamic ^1H NMR spectroscopy in CD_3SOCD_3. Although the rates of the ring interconversion[51] between these conforma-

tional diastereoisomers are slow on the ^{1}H NMR time scale at room temperature (298 K), the broadening of the signals for the aromatic protons in spectra recorded (Figures 6c and S15) between 308 and 418 K indicates that the rate of ring interconversion becomes increasingly fast at these elevated temperatures. A sequence of coalescence temperatures is observed[52] in the temperature range from 348 to 408 K, indicating that the free energies of activation for the interconversion between the two diastereoisomers are less than 20 kcal mol^{-1}. We observed no change in the ^{1}H NMR spectra (Figure S16) of **R-2BTDI** on cooling a DMF-d_7 solution down to 248 K, indicating that **R-Diastereoisomer-1** and **R-Diastereoisomer-2** are the only two diastereoisomeric conformations observable by dynamic ^{1}H NMR spectroscopy.

By contrast, the ^{1}H NMR spectrum (Figure S7) of **R-2BPDI** in CDCl$_3$ exhibits two doublets and one singlet in the range of δ 7.02−7.94 ppm, which represent a single conformational diastereoisomer. Dynamic ^{1}H NMR spectroscopy (Figure S17) in DMF-d_7 indicates the existence of only one stable conformational diastereoisomer in solution, a conclusion supported by the ^{13}C NMR spectrum (Figure S8) of **R-2BPDI** recorded in CDCl$_3$.

UV/Vis Spectroscopy and Circular Dichroism. The absorption spectrum (Figure 7a) of **R-2BTDI** exhibits three characteristic absorption peaks with maxima at 220, 258, and 307 nm. Figure 7b illustrates the chiral specific Cotton effects generated by the interchromophoric exciton coupling of the
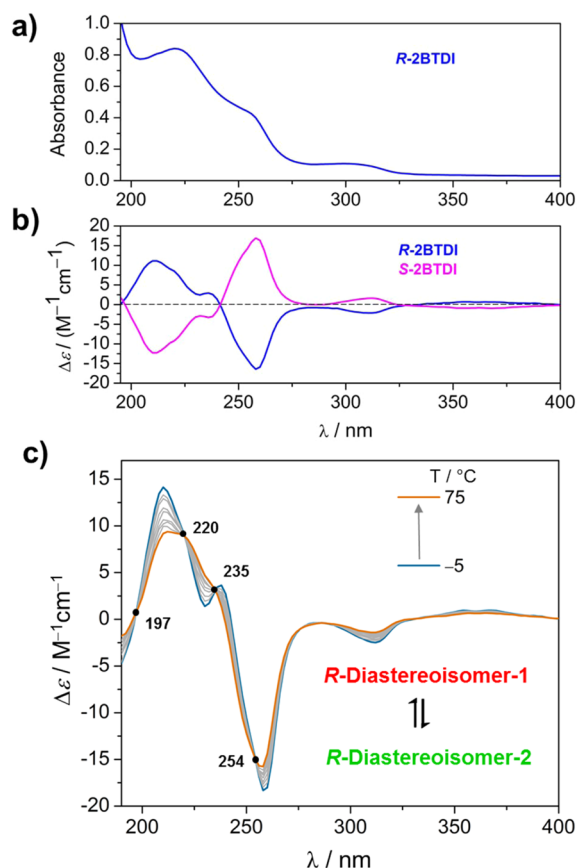
Figure 7. (a) UV/Vis absorption spectrum of **R-2BTDI** in MeCN at 298 K. (b) CD spectra of **R-2BTDI** (in blue) and **S-2BTDI** (in magenta) in MeCN at 298 K. (c) VT CD spectra of **R-2BTDI** in MeCN. The isosbestic points are indicated with black dots.

neighboring BTDI subunits in **R-2BTDI** and **S-2BTDI**.[53] The enantiomers **R-2BTDI** and **S-2BTDI** exhibit perfectly mirror-imaged CD spectra in MeCN. Variable-temperature circular dichroism (VT CD) was performed (Figure 7c) in MeCN in order to investigate the conformational interconversion between the diastereoisomers of **R-2BTDI**. It should be noted that a significant decrease in the intensities of the CD signals is observed upon heating the solution of **R-2BTDI** from −5 to 75 °C. Furthermore, the VT CD spectra of **R-2BTDI** exhibit four isosbestic points at 197, 220, 235, and 254 nm, indicating that (i) only two diastereoisomers are participating in the conformational equilibration and (ii) the ratio between two conformational diastereoisomers is changing with temperature. These observations are in good agreement with the results obtained by NMR spectroscopy. Neither isosbestic points nor changes in the intensities of CD signals were observed (Figure S18) in the VT CD of **R-2BPDI**, confirming its existence in MeCN solution as a single conformational diastereoisomer.

Density Functional Theory Structure Optimization. In order to gain better insight into the experimental results, density functional theory (DFT) structure optimization of **R-2BTDI** in DMSO was performed using the Perdew−Burke−Ernzerhof[54] (PBE) type of GGA exchange-correlation function and the 6-311G** basis set. Dispersion interactions were included using Grimme's empirical potential,[55] and solvation was described via the CPCM model.[56] Two different conformations (Figure S19), which are superimposable upon **R-Diastereoisomer-1** (**dduddu**) and **R-Diastereoisomer-2** (**uduudu**), with very similar energies were identified. The "dihedral angles" of the phenylene rings with respect to the ketonic C=O groups and the distance between the ketonic C=O groups for both diastereoisomers are similar to those in their solid-state structures. The calculated energy corresponding to **R-Diastereoisomer-1** is only 0.25 kcal mol^{-1} more stable than that for **R-Diastereoisomer-2**. This small difference in energy (ΔE) is in agreement with the slightly higher population of **R-Diastereoisomer-1** over **R-Diastereoisomer-2** in solution. Indeed, the calculated Boltzmann ratio of populations for the two conformations (approximately $e^{-\Delta E/kT}$, where ΔE is the energy difference) is ∼1.5:1 for the two diastereoisomeric conformations, in excellent agreement with the experimental results.

Electrochemistry. Cyclic voltammetry (CV) was performed (Figure 8) in THF on the building blocks of the helices formed by **R-2BTDI**, and the results were compared with those for **R-2BPDI** as well as for the reference compounds, **BTDI-ref** and **BPDI-ref**. The CV of **BTDI-ref** shows (Figure 8a) three distinct reversible one-electron waves with peak potentials at −1064, −1402, and −1941 mV, corresponding to the formation of the [**BTDI-ref**]$^{•−}$ radical anion, the [**BTDI-ref**]$^{2−}$ dianion, and the [**BTDI-ref**]$^{•−/2−}$ radical anion/dianion, respectively. On the other hand, the CV of **R-2BTDI** displays (Figure 8a) multiple reduction processes involving a total of six electrons—namely, (i) two consecutive one-electron reduction waves (broad) at −1047 and −1170 mV, corresponding to the formation of the [**R-2BTDI**]$^{2(•−)}$ di(radical anion), (ii) two subsequent reversible one-electron waves (broad) at −1552 and −1734 mV, corresponding to the reduction of the two ketonic C=O groups resulting in a tetraanion species [**R-2BTDI**]$^{4−}$, and finally, (iii) a quasi-reversible two-electron process at −2031 mV, corresponding to the formation of an [**R-2BTDI**]$^{2(•−)/4−}$ di(radical anion)/tetraanion. It is expected that the equilibration between **R-**
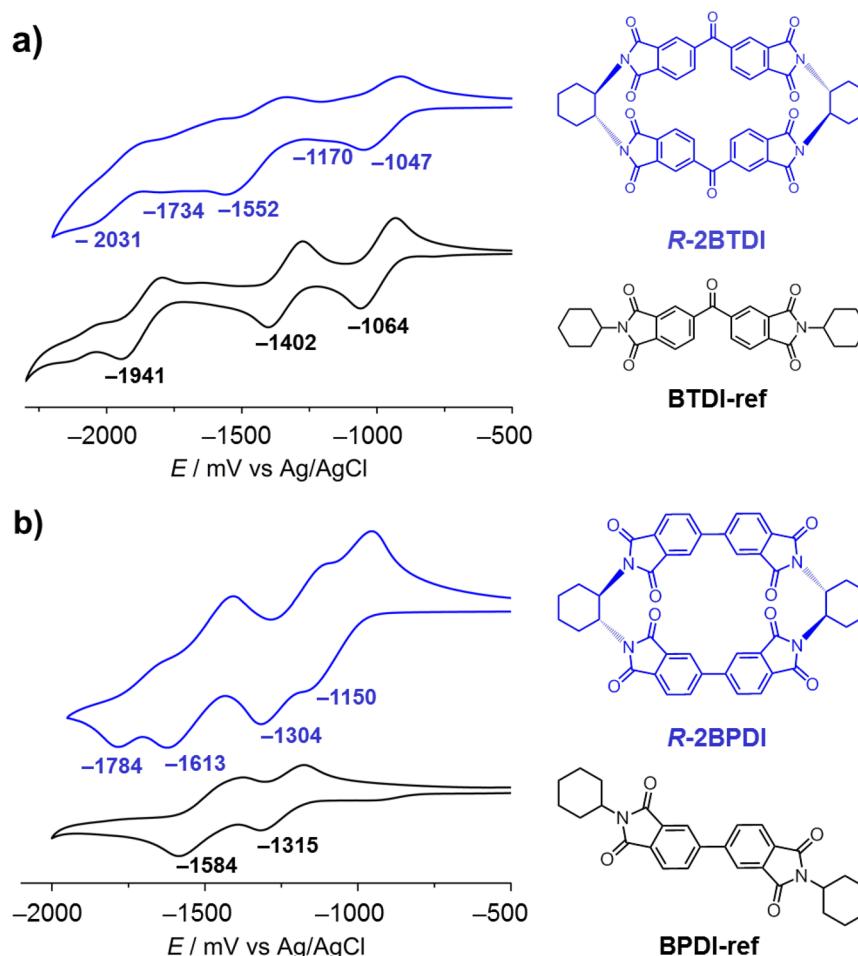
Figure 8. Electrochemical characterization. Solution-state CVs (1 mM in THF, 100 mM TBAPF$_6$, 50 mV s^{-1}, 298 K) of **BTDI-ref**, **R-2BTDI**, **BPDI-ref**, and **R-2BPDI**. Reduction peak potentials (E_{Red}) are displayed on the CVs.

Diasteroisomer-1 and **R-Diasteroisomer-2** causes the broadening of the reduction waves in solution. Moreover, the CV of **BPDI-ref** is characterized (Figure 8b) by two sequential one-electron cathodic waves, observed at −1315 and −1584 mV, corresponding to the formation of the [**BPDI-ref**]$^{•−}$ radical anion and the [**BPDI-ref**]$^{2−}$ dianion, respectively. By contrast, the CV of **R-2BPDI** shows four well-separated reversible one-electron waves. The first reduction potential (E_1 = −1150 mV) is shifted by 165 mV toward more positive potential compared with that (E_1 = −1315 mV) of **BPDI-ref**, while the second one of **R-2BPDI** (E_2 = −1304 mV) is shifted by only 11 mV. Conversely, the last two reduction potentials of **R-2BPDI** (E_3/E_4 = −1613/−1784 mV) are shifted toward more negative potentials compared with those for **BPDI-ref**. The observations from the comparative CV measurements of both the dimers highlight the facts that (i) the first reduction potential of the BTDI unit in the **R-2BTDI** is shifted by 20 mV toward more positive potentials compared with that of **BTDI-ref**, whereas this shift is large (~165 mV) in **R-2BPDI**, and (ii) the first two reduction waves in **R-2BTDI** separate into four reversible one-electron waves, which are not as distinctive as in **R-2BPDI**. The redox behavior of the dimers indicates that the electronic communication between the two equivalent BPDI redox units in **R-2BPDI** as a result of the mixing of their π-orbitals is much more pronounced than that of the BTDI units in **R-2BTDI**. We have shown previously[35] that the rigidity and small (<4.5 Å) interplanar distances are the most significant

parameters when it comes to attaining effective through-space electronic communication in cyclophanes. The inefficient through-space electronic communication (hence peak broadening) in **R-2BTDI** could be a consequence of the equilibration between **R-Diasteroisomer-1** and **R-Diasteroisomer-2**, with interplanar distances between the two ketonic C=O groups of 8.2 and 5.2 Å, respectively. By contrast, the rigid **R-2BPDI**, with a distance of 4.6 Å between the two BPDI units, shows effective cyclical through-space electron sharing.

■ CONCLUSIONS

In summary, two enantiopure macrocyclic dimers, **R-2BTDI** and **R-2BPDI**, along with their enantiomers, have been synthesized. Comparison of the (^{1}H and ^{13}C) NMR and CD spectra of these dimers in solution reveals that **R-2BTDI** exists at room temperature in two diastereoisomeric conformations of comparable energies, as indicated by both experiments and DFT calculations. The molar ratio of the major conformational diastereoisomer to the minor one in CD$_3$SOCD$_3$ solution is 1.5:1, based on integration of their separate signals observed in the ^{1}H NMR spectrum at room temperature. Crystallization of **R-2BTDI** from a mixed-solvent system leads to the formation of a double-helical superstructure incorporating an equimolar ratio of these two diastereoisomeric conformations, stabilized by multiple [C−H⋯O] and π−π stacking interactions in the solid state. Single-crystal XRD analysis reveals the operation of a self-sorting system in the formation of a double helix with a

helical pitch of 4.06 nm composed of eight macrocycles, including four of each conformational diastereoisomer. The high yield from the crystallization of **R-2BTDI** indicates that the diastereoisomers are equilibrating during the crystallization process. The helical sense of the superstructure depends on the absolute configurations of the four stereogenic centers present in the macrocyclic dimers. A right-handed double helix is observed when starting from **R-2BTDI** and a left-handed one when starting from **S-2BTDI**. Interconversion of the two conformational diastereoisomers in CD_3SOCD_3 solution leads to broadening of the resonances for their BTDI protons undergoing site exchange in the temperature range of 298−418 K in the ^1H NMR spectra. The activation barrier associated with this conformational interconversion between the diastereoisomers is estimated to be in the high teens of kcal mol^{-1}. The occurrence of isosbestic points in the VT CD spectra in acetonitrile confirms the existence of two interconverting conformational diastereoisomers, the ratios of which vary with temperature. On the other hand, **R-2BPDI** exists in only one diastereoisomeric conformation, as confirmed by NMR spectroscopy in $CDCl_3$ solution. X-ray crystallography of a single crystal grown from a mixed-solvent system indicates the existence of only a single conformational diastereoisomer in the solid state. We speculate that the ketonic C=O groups of the BTDI units in **R-2BTDI** and **S-2BTDI** provide sufficient conformational flexibility, unlike the BPDI units in **R-2BPDI**, to support the formation of the two stable conformational diastereoisomers both in solution and in the solid state. Moreover, the results from CV indicate the presence of through-space orbital interactions and the associated electron-sharing phenomena in both redox-active, dimeric **R-2BTDI** and **R-2BPDI**. The assembly of a double-helical superstructure, composed of two conformational diastereoisomeric building blocks in the case of **R-2BTDI**, constitutes a rare emergent example of *social self-sorting*.

ASSOCIATED CONTENT

Ⓢ Supporting Information

The Supporting Information is available free of charge on the ACS Publications website at DOI: 10.1021/jacs.6b09258.

X-ray crystallographic data for **R-2BPDI** (CIF)
X-ray crystallographic data for **R-2BTDI** (CIF)
X-ray crystallographic data for **S-2BTDI** (CIF)
Experimental details and characterization data, including syntheses, NMR spectra, Schemes S1−S6, Figures S1−S19, and Tables S1 and S2 (PDF)

AUTHOR INFORMATION

Corresponding Author
*stoddart@northwestern.edu

Author Contributions
[#]A.S. and Z.L. contributed equally to this work.

Notes
The authors declare no competing financial interest.

ACKNOWLEDGMENTS

REFERENCES

(1) Schattschneider, D. *Sci. Am.* **1994**, *271*, 66.
(2) Kratschmer, W.; Lamb, L. D.; Fostiropoulos, K.; Huffman, D. R. *Nature* **1990**, *347*, 354.
(3) (a) Barnes, C. P.; Sell, S. A.; Boland, E. D.; Simpson, D. G.; Bowlin, G. L. *Adv. Drug Delivery Rev.* **2007**, *59*, 1413. (b) Sun, H.; Meng, F.; Dias, A. A.; Hendriks, M.; Feijen, J.; Zhong, Z. *Biomacromolecules* **2011**, *12*, 1937. (c) Samanta, A.; Tesch, M.; Keller, U.; Klingauf, J. r.; Studer, A.; Ravoo, B. J. *J. Am. Chem. Soc.* **2015**, *137*, 1967. (d) Tu, Y.; Peng, F.; Adawy, A.; Men, Y.; Abdelmohsen, L. K. E. A.; Wilson, D. A. *Chem. Rev.* **2016**, *116*, 2023.
(4) (a) Eigen, M. *Naturwissenschaften* **1971**, *58*, 465. (b) Newth, D.; Finnigan, J. *Aust. J. Chem.* **2006**, *59*, 841. (c) Buck, M. R.; Bondi, J. F.; Schaak, R. E. *Nat. Chem.* **2012**, *4*, 37. (d) Angille, M. R.; Zhang, J.; Personick, M. L.; Li, S.; Mirkin, C. A. *Science* **2012**, *337*, 954. (e) McHale, R.; Patterson, J. P.; Zetterlund, P. B.; O'Reilly, R. K. *Nat. Chem.* **2012**, *4*, 491. (f) Lehn, J.-M. *Angew. Chem., Int. Ed.* **2013**, *52*, 2836. (g) Samanta, A.; Ravoo, B. J. *Angew. Chem., Int. Ed.* **2014**, *53*, 12946. (h) Somiya, M.; Kuroda, S. i. *Adv. Drug Delivery Rev.* **2015**, *95*, 77. (i) Kincer, M. R.; Choudhury, R.; Srinivasarao, M.; Beckham, H. W.; Briggs, G. A. D.; Porfyrakis, K.; Bucknall, D. G. *Polymer* **2015**, *56*, 516. (j) Zhang, Y.; Gong, S.; Zhang, Q.; Ming, P.; Wan, S.; Peng, J.; Jiang, L.; Cheng, Q. *Chem. Soc. Rev.* **2016**, *45*, 2378. (k) Bisoyi, H. K.; Li, Q. *Angew. Chem., Int. Ed.* **2016**, *55*, 2994. (l) Choi, Y.-J.; Kim, D.-Y.; Park, M.; Yoon, W.-J.; Lee, Y.; Hwang, J.-K.; Chiang, Y.-W.; Kuo, S.-W.; Hsu, C.-H.; Jeong, K.-U. *ACS Appl. Mater. Interfaces* **2016**, *8*, 9490.
(5) (a) Albrecht, M. *Chem. Rev.* **2001**, *101*, 3457. (b) Albrecht, M. *Angew. Chem., Int. Ed.* **2005**, *44*, 6448.
(6) Pauling, L.; Corey, R. B.; Branson, H. R. *Proc. Natl. Acad. Sci. U. S. A.* **1951**, *37*, 205.
(7) Watson, J. D.; Crick, F. H. *Nature* **1953**, *171*, 737.
(8) (a) Iijima, S. *Nature* **1991**, *354*, 56. (b) Green, M. M.; Peterson, N. C.; Sato, T.; Teramoto, A.; Cook, R.; Lifson, S. *Science* **1995**, *268*, 1860. (c) Engelkamp, H.; Middelbeek, S. *Science* **1999**, *284*, 785. (d) Green, M. M.; Park, J. W.; Sato, T.; Teramoto, A.; Lifson, S.; Selinger, R. L.; Selinger, J. V. *Angew. Chem., Int. Ed.* **1999**, *38*, 3138. (e) Natansohn, A.; Rochon, P. *Chem. Rev.* **2002**, *102*, 4139. (f) Maeda, K.; Yashima, E. *Top. Curr. Chem.* **2006**, *265*, 47. (g) Palmans, A. R.; Meijer, E. W. *Angew. Chem., Int. Ed.* **2007**, *46*, 8948. (h) Furusho, Y.; Yashima, E. *J. Polym. Sci., Part A: Polym. Chem.* **2009**, *47*, 5195. (i) Seoudi, R. S.; Del Borgo, M. P.; Kulkarni, K.; Perlmutter, P.; Aguilar, M.-I.; Mechler, A. *New J. Chem.* **2015**, *39*, 3280. (j) Anuradha, A.; La, D. D.; Al Kobaisi, M.; Bhosale, S. V. *Sci. Rep.* **2015**, *5*, 15652.
(9) (a) Hasenknopf, B.; Lehn, J.-M.; Baum, G.; Fenske, D. *Proc. Natl. Acad. Sci. U. S. A.* **1996**, *93*, 1397. (b) Tanaka, Y.; Katagiri, H.; Furusho, Y.; Yashima, E. *Angew. Chem., Int. Ed.* **2005**, *44*, 3867. (c) Zhao, J. a.; Mi, L.; Hu, J.; Hou, H.; Fan, Y. *J. Am. Chem. Soc.* **2008**, *130*, 15222. (d) Lim, Y. b.; Lee, E.; Yoon, Y. R.; Lee, M. S.; Lee, M. *Angew. Chem., Int. Ed.* **2008**, *47*, 4525.
(10) Lin, Y.; Mao, C. *Front. Mater. Sci.* **2011**, *5*, 247.
(11) (a) Lehn, J.-M.; Rigault, A.; Siegel, J.; Harrowfield, J.; Chevrier, B.; Moras, D. *Proc. Natl. Acad. Sci. U. S. A.* **1987**, *84*, 2565. (b) Koert, U.; Harding, M. M.; Lehn, J.-M. *Nature* **1990**, *346*, 339. (c) Woods, C. R.; Benaglia, M.; Siegel, J. S.; Cozzi, F. *Angew. Chem., Int. Ed. Engl.* **1996**, *35*, 1830. (d) Piguet, C.; Bernardinelli, G.; Hopfgartner, G. *Chem. Rev.* **1997**, *97*, 2005. (e) Hill, D. J.; Mio, M. J.; Prince, R. B.; Hughes, T. S.; Moore, J. S. *Chem. Rev.* **2001**, *101*, 3893. (f) Orita, A.; Nakano, T.; An, D. L.; Tanikawa, K.; Wakamatsu, K.; Otera, J. *J. Am. Chem. Soc.* **2004**, *126*, 10389. (g) Stephenson, A.; Ward, M. D. *Chem. Commun.* **2012**, *48*, 3605. (h) Boer, S. A.; Turner, D. R. *Chem. Commun.* **2015**, *51*, 17375. (i) Nakamura, T.; Kimura, H.; Okuhara, T.; Yamamura, M.; Nabeshima, T. *J. Am. Chem. Soc.* **2016**, *138*, 794.
(12) (a) Sánchez-Quesada, J.; Seel, C.; Prados, P.; de Mendoza, J.; Dalcol, I.; Giralt, E. *J. Am. Chem. Soc.* **1996**, *118*, 277. (b) Gong, B.;

Yan, Y.; Zeng, H.; Skrzypczak-Jankunn, E.; Kim, Y. W.; Zhu, J.; Ickes, H. *J. Am. Chem. Soc.* **1999**, *121*, 5607. (c) Berl, V.; Huc, I.; Khoury, R. G.; Krische, M. J.; Lehn, J.-M. *Nature* **2000**, *407*, 720. (d) Bisson, A. P.; Carver, F. J.; Eggleston, D. S.; Haltiwanger, R. C.; Hunter, C. A.; Livingstone, D. L.; McCabe, J. F.; Rotger, C.; Rowan, A. E. *J. Am. Chem. Soc.* **2000**, *122*, 8856. (e) Zeng, H.; Miller, R. S.; Flowers, R. A.; Gong, B. *J. Am. Chem. Soc.* **2000**, *122*, 2635.

(13) (a) Kumaki, J.; Kawauchi, T.; Yashima, E. *J. Am. Chem. Soc.* **2005**, *127*, 5788. (b) Goto, H.; Furusho, Y.; Miwa, K.; Yashima, E. *J. Am. Chem. Soc.* **2009**, *131*, 4710. (c) Goto, H.; Katagiri, H.; Furusho, Y.; Yashima, E. *J. Am. Chem. Soc.* **2006**, *128*, 7176.

(14) (a) Rickhaus, M.; Bannwart, L. M.; Neuburger, M.; Gsellinger, H.; Zimmermann, K.; Häussinger, D.; Mayor, M. *Angew. Chem., Int. Ed.* **2014**, *53*, 14587. (b) Gidron, O.; Ebert, M. O.; Trapp, N.; Diederich, F. *Angew. Chem., Int. Ed.* **2014**, *53*, 13614. (c) Rickhaus, M.; Mayor, M.; Juríček, M. *Chem. Soc. Rev.* **2016**, *45*, 1542.

(15) Lehn, J.-M. *Supramolecular Chemistry: Concept and Perspective*; VCH: Weinheim, Germany, 1995.

(16) (a) Amabilino, D. B.; Stoddart, J. F. *Chem. Rev.* **1995**, *95*, 2725. (b) Conn, M. M.; Rebek, J., Jr. *Chem. Rev.* **1997**, *97*, 1647. (c) Pan, G.-B.; Cheng, X.-H.; Höger, S.; Freyland, W. *J. Am. Chem. Soc.* **2006**, *128*, 4218.

(17) Schneebeli, S. T.; Frasconi, M.; Liu, Z.; Wu, Y.; Gardner, D. M.; Strutt, N. L.; Cheng, C.; Carmieli, R.; Wasielewski, M. R.; Stoddart, J. F. *Angew. Chem., Int. Ed.* **2013**, *52*, 13100.

(18) (a) Liu, M.; Zhang, L.; Wang, T. *Chem. Rev.* **2015**, *115*, 7304. (b) Zhang, X.; Li, B.; Zhang, J. *Inorg. Chem.* **2016**, *55*, 3378.

(19) Pasteur, L. *Ann. Chim. Phys.* **1848**, *24*, 442.

(20) (a) Anderson, L.; Hill, D. W. *J. Chem. Soc.* **1928**, 993. (b) Pérez-García, L.; Amabilino, D. B. *Chem. Soc. Rev.* **2002**, *31*, 342.

(21) Viedma, C. *Phys. Rev. Lett.* **2005**, *94*, 065504.

(22) Haq, S.; Liu, N.; Humblot, V.; Jansen, A.; Raval, R. *Nat. Chem.* **2009**, *1*, 409.

(23) Pérez-García, L.; Amabilino, D. B. *Chem. Soc. Rev.* **2007**, *36*, 941.

(24) (a) Wu, A.; Isaacs, L. *J. Am. Chem. Soc.* **2003**, *125*, 4831. (b) Mukhopadhyay, P.; Wu, A.; Isaacs, L. *J. Org. Chem.* **2004**, *69*, 6157. (c) Safont-Sempere, M. M.; Fernández, G.; Würthner, F. *Chem. Rev.* **2011**, *111*, 5784. (d) Yan, L.-L.; Tan, C.-H.; Zhang, G.-L.; Zhou, L.-P.; Bünzli, J.-C.; Sun, Q.-F. *J. Am. Chem. Soc.* **2015**, *137*, 8550. (e) Sandeep, A.; Praveen, V. K.; Kartha, K. K.; Karunakaran, V.; Ajayaghosh, A. *Chem. Sci.* **2016**, *7*, 4460.

(25) (a) Shivanyuk, A.; Rebek, J., Jr. *J. Am. Chem. Soc.* **2002**, *124*, 12074. (b) Li, L.; Zhang, H. Y.; Zhao, J.; Li, N.; Liu, Y. *Chem. - Eur. J.* **2013**, *19*, 6498. (c) Joseph, R.; Nkrumah, A.; Clark, R. J.; Masson, E. *J. Am. Chem. Soc.* **2014**, *136*, 6602. (d) Benkhäuser, C.; Lützen, A. *Beilstein J. Org. Chem.* **2015**, *11*, 693.

(26) (a) Taylor, P. N.; Anderson, H. L. *J. Am. Chem. Soc.* **1999**, *121*, 11538. (b) Gidron, O.; Jirásek, M.; Trapp, N.; Ebert, M.-O.; Zhang, X.; Diederich, F. *J. Am. Chem. Soc.* **2015**, *137*, 12502. (c) Johnson, A. M.; Wiley, C. A.; Young, M. C.; Zhang, X.; Lyon, Y.; Julian, R. R.; Hooley, R. J. *Angew. Chem., Int. Ed.* **2015**, *54*, 5641.

(27) (a) Jolliffe, K. A.; Timmerman, P.; Reinhoudt, D. N. *Angew. Chem., Int. Ed.* **1999**, *38*, 933. (b) Corbin, P. S.; Lawless, L. J.; Li, Z.; Ma, Y.; Witmer, M. J.; Zimmerman, S. C. *Proc. Natl. Acad. Sci. U. S. A.* **2002**, *99*, 5099. (c) Ma, Y.; Kolotuchin, S. V.; Zimmerman, S. C. *J. Am. Chem. Soc.* **2002**, *124*, 13757.

(28) (a) Shaller, A. D.; Wang, W.; Gan, H.; Li, A. D. Q. *Angew. Chem., Int. Ed.* **2008**, *47*, 7705. (b) Safont-Sempere, M. M.; Osswald, P.; Stolte, M.; Grüne, M.; Renz, M.; Kaupp, M.; Radacki, K.; Braunschweig, H.; Würthner, F. *J. Am. Chem. Soc.* **2011**, *133*, 9580.

(29) (a) Sun, Q.-F.; Iwasa, J.; Ogawa, D.; Ishido, Y.; Sato, S.; Ozeki, T.; Sei, Y.; Yamaguchi, K.; Fujita, M. *Science* **2010**, *328*, 1144. (b) Kumar, D. K.; Steed, J. W. *Chem. Soc. Rev.* **2014**, *43*, 2080. (c) Yoon, B.; Luedtke, W.; Barnett, R. N.; Gao, J.; Desireddy, A.; Conn, B. E.; Bigioni, T.; Landman, U. *Nat. Mater.* **2014**, *13*, 807.

(30) (a) Prince, R. B.; Brunsveld, L.; Meijer, E. W.; Moore, J. S. *Angew. Chem., Int. Ed.* **2000**, *39*, 228. (b) Miyauchi, M.; Takashima, Y.; Yamaguchi, H.; Harada, A. *J. Am. Chem. Soc.* **2005**, *127*, 2984. (c) Dolain, C.; Jiang, H.; Léger, J.-M.; Guionneau, P.; Huc, I. *J. Am.*

Chem. Soc. **2005**, *127*, 12943. (d) Amabilino, D. B.; Veciana, J. *Top Curr. Chem.* **2006**, *265*, 253. (e) Brizard, A.; Aimé, C.; Labrot, T.; Huc, I.; Berthier, D.; Artzner, F.; Desbat, B.; Oda, R. *J. Am. Chem. Soc.* **2007**, *129*, 3754. (f) Pijper, D.; Jongejan, M. G.; Meetsma, A.; Feringa, B. L. *J. Am. Chem. Soc.* **2008**, *130*, 4541. (g) Nagata, Y.; Nishikawa, T.; Suginome, M. *ACS Macro Lett.* **2016**, *5*, 519. (h) Xiao, W.; Ernst, K.-H.; Palotas, K.; Zhang, Y.; Bruyer, E.; Peng, L.; Greber, T.; Hofer, W. A.; Scott, L. T.; Fasel, R. *Nat. Chem.* **2016**, *8*, 326.

(31) Kim, Y. K.; Lee, J. M.; Park, H. B.; Lee, Y. M. *J. Membr. Sci.* **2004**, *235*, 139.

(32) Atai, M.; Nekoomanesh, M.; Hashemi, S. A.; Amani, S. *Dent. Mater.* **2004**, *20*, 663.

(33) Delozier, D. M.; Orwoll, R. A.; Cahoon, J. F.; Johnston, N. J.; Smith, J. G., Jr.; Connell, J. W. *Polymer* **2002**, *43*, 813.

(34) Hou, A.; Feng, G.; Zhuo, J.; Sun, G. *ACS Appl. Mater. Interfaces* **2015**, *7*, 27918.

(35) Wu, Y.; Frasconi, M.; Gardner, D. M.; McGonigal, P. R.; Schneebeli, S. T.; Wasielewski, M. R.; Stoddart, J. F. *Angew. Chem., Int. Ed.* **2014**, *53*, 9476.

(36) Nalluri, S. K. M.; Liu, Z.; Wu, Y.; Hermann, K. R.; Samanta, A.; Kim, D. J.; Krzyaniak, M. D.; Wasielewski, M. R.; Stoddart, J. F. *J. Am. Chem. Soc.* **2016**, *138*, 5968.

(37) Wu, Y.; Nalluri, S. K. M.; Young, R. M.; Krzyaniak, M. D.; Margulies, E. A.; Stoddart, J. F.; Wasielewski, M. R. *Angew. Chem., Int. Ed.* **2015**, *54*, 11971.

(38) (a) Tans, S. J.; Verschueren, A. R.; Dekker, C. *Nature* **1998**, *393*, 49. (b) Coropceanu, V.; Cornil, J.; da Silva Filho, D. A.; Olivier, Y.; Silbey, R.; Brédas, J.-L. *Chem. Rev.* **2007**, *107*, 926. (c) Kiguchi, M.; Takahashi, T.; Takahashi, Y.; Yamauchi, Y.; Murase, T.; Fujita, M.; Tada, T.; Watanabe, S. *Angew. Chem., Int. Ed.* **2011**, *50*, 5708. (d) Saeki, A.; Koizumi, Y.; Aida, T.; Seki, S. *Acc. Chem. Res.* **2012**, *45*, 1193.

(39) Crystal data for **R-2BPDI** (see Supporting Information, including CIF file): monoclinic, space group *C2* (no. 5), a = 32.045(4), b = 8.2580(9), and c = 14.0706(15) Å, β = 97.500(3)°, V = 3691.6(7) Å^3, Z = 4, T = 99.99 K, μ(Cu Kα) = 0.812 mm^{-1}, D_{calc} = 1.398 g/mm^3, 19 174 reflections measured (6.336 ≤ 2θ ≤ 130.358), 6201 unique (R_{int} = 0.0377, R_{sigma} = 0.0421) which were used in all calculations. The final R_1 was 0.0372 ($I > 2\sigma(I)$), and wR_2 was 0.1008 (all data). CCDC 1485203 also contains the supplementary crystallographic data for this paper. These data can be obtained free of charge from The Cambridge Crystallographic Data Centre via www.ccdc.cam.ac.uk/data_request/cif.

(40) Crystal data for **R-2BTDI** (see Supporting Information, including CIF file): tetragonal, space group *P4₁22* (no. 91), a = 15.4764(5), c = 40.5896(19) Å, V = 9722.0(8) Å^3, Z = 8, T = 99.99 K, μ(Cu Kα) = 1.691 mm^{-1}, D_{calc} = 1.229 g/mm^3, 17 999 reflections measured (5.71 ≤ 2θ ≤ 100.872), 5096 unique (R_{int} = 0.0960, R_{sigma} = 0.0923) which were used in all calculations. The final R_1 was 0.0768 ($I > 2\sigma(I)$), and wR_2 was 0.2251 (all data). CCDC 1485202 also contains the supplementary crystallographic data for this paper. These data can be obtained free of charge from The Cambridge Crystallographic Data Centre via www.ccdc.cam.ac.uk/data_request/cif.

(41) The *syn* orientation in the case of **R-Diastereoisomer-1** corresponds to the conformation where the isolated *ortho* hydrogen atoms (H_{1C}) on the four phenylene rings are pointing in the same direction. The "dihedral angle" denotes the angle between the planes of the two benzoimide units in the BTDI linkers.

(42) The *anti* orientation in the case of **R-Diastereoisomer-2** corresponds to the conformation where the two pairs of isolated *ortho* hydrogen atoms (H_{1C}) on the phenylene rings in the BTDI linkers are pointing in opposite directions.

(43) There are numerous solid-state structures reported for benzophenone in the literature. See: (a) Fleischer, E. B.; Sung, N.; Hawkinson, S. *J. Phys. Chem.* **1968**, *72*, 4311. (b) Kutzke, H.; Klapper, H.; Hammond, R. B.; Roberts, K. J. *Acta Crystallogr., Sect. B: Struct. Sci.* **2000**, *56*, 486. (c) Hammond, R. B.; Pencheva, K.; Roberts, K. J. *Faraday Discuss.* **2007**, *136*, 91. (d) Davey, R. J.; Schroeder, S. L.; ter Horst, J. H. *Angew. Chem., Int. Ed.* **2013**, *52*, 2166. (e) Reilly, A. M.;

Wann, D. A.; Gutmann, M. J.; Jura, M.; Morrison, C. A.; Rankin, D. W. H. *J. Appl. Crystallogr.* **2013**, *46*, 656. We have chosen the solid-state structure of benzophenone reported in ref (a) to compare the torsional angles with the diastereoisomers of *R*-2BTDI for the simple reason that the crystals were grown in same solvent system.

(44) The two helical strands in DNA entwine around the same axis to form a double helix with a diameter of ~2 nm and a pitch of 3.4 nm involving ~11 base pairs through complementary hydrogen bonds between the nucleotides and the $\pi-\pi$ stacking between the base pairs. In this paper, we report a unique artificial supramolecular analogue of double-helical DNA constructed from two complementary conformational diastereoisomers of a chiral macrocycle by means of similar noncovalent bonding interactions.

(45) Crystal data for *S*-2BTDI (see Supporting Information, including CIF file): tetragonal, $P4_322$ (No. 95), $a = 15.4749(5)$, $c = 40.5132(15)$ Å, $V = 9701.8(7)$ Å^3, $T = 100(2)$ K, $Z = 8$, $Z' = 1$, μ(Cu Kα) = 1.173, 32 085 reflections measured, 5113 unique ($R_{int} = 0.0913$), which were used in all calculations. The final wR_2 was 0.2880 (all data), and R_1 was 0.0918 ($I > 2\sigma(I)$). CCDC 1485201 also contains the supplementary crystallographic data for this paper. These data can be obtained free of charge from The Cambridge Crystallographic Data Centre via www.ccdc.cam.ac.uk/data_request/cif.

(46) In the conformational analysis of *R*-2BTDI, 64 possible conformations were obtained initially by permutating the relative orientations of the H_{1C} protons with respect to the O atoms on the ketonic C=O groups. After taking degeneracy about the C_2^z and C_2^y axes in account, 20 discrete conformational diastereoisomers were identified. There is no C_2^x axis present in either of the two conformational diastereoisomers.

(47) Conformational diastereoisomerism of this kind has also been observed in pillar[*n*]arenes (Strutt, N. L.; Zhang, H.; Schneebeli, S. T.; Stoddart, J. F. *Acc. Chem. Res.* **2014**, *47*, 2631−2642.) and calixarenes (Wang, M.-X. *Chem. Commun.* **2008**, 4541−4551.). The coexistence of discrete conformational diastereoisomers in homochiral macrocycles in both the solution phase and solid state is quite unique.

(48) (a) Gellatly, R. P.; Ollis, W. D.; Sutherland, I. O. *J. Chem. Soc., Perkin Trans. 1* **1976**, *1*, 913. (b) Hoorfar, A.; Ollis, W. D.; Stoddart, J. F. *J. Chem. Soc., Perkin Trans. 1* **1982**, *1*, 1721.

(49) The H_{1C} protons in the **dduddu** (*R*-Diastereoisomer-1) on the four phenylene rings are pointing in the opposite direction with respect to the ketonic C=O groups, resulting in their being less deshielding and hence shifted upfield in its ^{1}H NMR spectrum with respect to the other phenylene ring protons.

(50) There are two pairs H_{1C} protons in the case of **uduudu** (*R*-Diastereoisomer-2) on the four phenylene rings. One of the pairs (H_x) of the H_{1C} protons is pointing in the same direction as the ketonic C=O groups, resulting in more deshielding and hence exhibiting downfield shifts with respect to the other phenylene ring protons. The other pair ($H_{x'}$) is pointing in the opposite direction to the ketonic C=O groups and so exhibits upfield shifts on account of diminished deshielding.

(51) The two diastereoisomers, *R*-2BTDI (*R*-Diastereoisomer-1 and *R*-Diastereoisomer-2), are interconverting rapidly on the laboratory time scale at room temperature, as evidenced by recording the ^{1}H NMR spectrum of a single crystal of *R*-2BTDI (where the molar ratio of the diastereoisomers is 1:1) in CD$_3$SOCD$_3$ at room temperature where the molar ratio of *R*-Diastereoisomer-1 over *R*-Diastereoisomer-2 was found to be 1.5:1 rather than 1:1, indicating that rapid equilibration (which takes place while dissolving the crystal) between the diastereoisomers occurs on the laboratory time scale. When we recorded an ^{1}H NMR spectrum of a single crystal of *R*-2BTDI dissolved at −60 °C in DMF-d_7, we also failed to observe a 1:1 molar ratio of the diastereoisomers on account of their rapid equilibration even at this low temperature.

(52) The kinetic and thermodynamic parameters associated with the interconversion of the two diastereoisomers of *R*-2BTDI which are directly related to the rotation of phenylene rings around the C(=O)−C···N−C axis were estimated by the peak separation observed ($\Delta\nu_{ex} \approx 517$ Hz) for the *R*-Diastereoisomer-2 protons (H_X and $H_{X'}$) at room temperature. The protons H_X and $H_{X'}$ were chosen for this calculation because these diastereotopic H_{1C} protons of *R*-Diastereoisomer-2 can undergo exchange, leading to line broadening. The rate constants k_c were calculated (Sutherland, I. O. *Annu. Rep. NMR Spectrosc.* **1972**, *4*, 71.) by employing the approximation that $k_c = \pi(\Delta\nu_{ex})/(2)^{1/2}$ and found to be 1148 s^{-1}. By using the Eyring equation, $\Delta G_c^{\#} = -RT_c \ln(k_c h/k_b T_c)$, in which R is the gas constant, h is Planck's constant, and k_b is Boltzmann's constant, this rate constant (k_c) corresponds to $\Delta G_c^{\#} \approx 13.27$, 15.6, 17.0, and 18.9 kcal mol^{-1} at $T_c = 298$, 348, 378, and 418 K, respectively.

(53) In the case of *R*-2BTDI, a characteristically strong negative excitonic Cotton effect is observed in the range 200−270 nm, and a positive Cotton effect is observed in the range 290−380 nm.

(54) Perdew, J. P.; Burke, K.; Ernzerhof, M. *Phys. Rev. Lett.* **1996**, *77*, 3865.

(55) Grimme, S. *J. Comput. Chem.* **2006**, *27*, 1787.

(56) Cossi, M.; Rega, N.; Scalmani, G.; Barone, V. *J. Comput. Chem.* **2003**, *24*, 669.